Evaluation of mitochondrial redox status and energy metabolism of X-irradiated HeLa cells by LC/UV, LC/MS/MS and ESR

Kumiko Yamamoto[a], Yoshinori Ikenaka[b], Takahiro Ichise[b], Tomoki Bo[a], Mayumi Ishizuka[b], Hironobu Yasui[c], Wakako Hiraoka[d], Tohru Yamamori[a], Osamu Inanami[a]

[a] Laboratory of Radiation Biology, Department of Applied Veterinary Sciences, Faculty of Veterinary Medicine, Hokkaido University, Sapporo, Japan

[b] Laboratory of Toxicology, Department of Environmental Veterinary Science, Faculty of Veterinary Medicine, Hokkaido University, Sapporo, Japan

[c] Central Institute of Isotope Science, Hokkaido University, Sapporo, Japan

[d] Laboratory of Biophysics, School of Science and Technology, Meiji University, Kawasaki, Japan

*Corresponding authors: Prof. Osamu Inanami

Address: Kita 18, Nishi 9, Kita-ku, Sapporo, Hokkaido 060-0818, Japan

Tel: +81-11-706-5235, Fax: +81-11-706-7373

E-mail: inanami@vetmed.hokudai.ac.jp

Running Head

Mitochondrial redox status in X-irradiated tumor

Abstract

To evaluate the metabolic responses in tumor cells exposed to ionizing radiation, oxygen consumption rate (OCR), cellular lipid peroxidation, cellular energy status (intracellular nucleotide pool and ATP production), and mitochondrial reactive oxygen species (ROS), semiquinone (SQ), and iron–sulfur (Fe–S) cluster levels were evaluated in human cervical carcinoma HeLa cells at 12 and 24 h after X-irradiation. LC/MS/MS analysis showed that levels of 8-iso $PGF_{2\alpha}$ and 5-i$PF_{2\alpha}$-VI, lipid peroxidation products of membrane arachidonic acids, were not altered significantly in X-irradiated cells, although mitochondrial ROS levels and OCR significantly increased in the cells at 24 h after irradiation. LC/UV analysis revealed that intracellular AMP, ADP, and ATP levels increased significantly after X-irradiation, but adenylate energy charge (AEC = [ATP + 0.5 × ADP]/[ATP + ADP + AMP]) remained unchanged after X-irradiation. In low-temperature electron spin resonance (ESR) spectra of HeLa cells, the presence of mitochondrial SQ at g = 2.004 and Fe–S cluster at g = 1.941 was observed and X-irradiation enhanced the signal intensity of SQ but not of the Fe–S cluster. Furthermore, this radiation-induced increase in SQ signal intensity disappeared on treatment with rotenone, which inhibits electron transfer from Fe–S cluster to SQ in complex I. From these results, it was suggested that an increase in OCR and imbalance in SQ and Fe–S cluster levels, which play a critical role in the mitochondrial electron transport chain (ETC), occur after X-irradiation, resulting in an increase in ATP production and ROS leakage from the activated mitochondrial ETC.

Keywords: electron spin resonance (ESR); tumor; mitochondrial electron transport chain (ETC); ionizing radiation; semiquinone; Fe–S cluster

Introduction

It is well-known that cancer cells tend to convert glucose into lactate for energy production rather than utilizing the mitochondrial electron transport chain (ETC), even under oxygenated conditions (i.e., the Warburg effect) [1]. Recently, it has been reported that most cancers still retain mitochondrial function [2] and inhibition of mitochondrial ETC stimulates the apoptotic signaling pathways [3]. Lu *et al*. showed a rapid relocation of the mammalian target of rapamycin (mTOR) to mitochondria and reprogramming of biogenetics from glycolysis to mitochondrial oxidative phosphorylation due to the mTOR-mediated inhibition of hexokinase II, a key enzyme in regulation of glycolysis, in tumor cells after irradiation [4]. In our recent studies [5,6], inhibition of dynamin-related protein 1 (Drp1), which controlled mitochondrial fission, reduced mitotic catastrophe in mouse fibroblast NIH3T3 cells and mouse SV40-immortalized embryo fibroblasts exposed to X-rays. It was also demonstrated that treatment with lipophilic triphenylphosphonium cation (TPP^+) derivatives, which inhibit mitochondrial ETC, enhanced X-ray-induced cell death by increasing reactive oxygen species (ROS) release from mitochondria and loss of intracellular ATP in human cervical carcinoma HeLa cells [7]. Compared to the cytotoxicity induced by cisplatin alone, enhanced cytotoxicity was observed when cisplatin was delivered to mitochondria of chemoresistant A2780/CP70 cells by nanoparticles (NP); the cisplatin-nanoparticle combination decreased mtDNA levels and mitochondrial function [8]. In contrast, 3-methyl pyruvate, an activating agent for mitochondrial ETC, enhances radiosensitivity by increasing mitochondria-derived ROS levels in human lung carcinoma A549 cells and murine squamous carcinoma SCCVII cells [9]. These reports strongly suggested mitochondria as novel targets for radiation and chemotherapy in tumor tissue.

Several reports have shown that delayed production of ROS from mitochondria is observed in human hepatocellular carcinoma HLE cells [10,11], HeLa cells [12,13], human umbilical vein endothelial cells (HUVECs) [14], human leukemic cells K562 cells [15,16], HL60 cells [16], normal human foreskin fibroblast BJ-hTERT cells [17], and Chinese hamster ovary cells [18] after exposure to ionizing radiation. Moreover, it has been reported that the antitumor genotoxic drugs cisplatin- [19] and doxorubicin-[20] induced ROS release from mitochondria is linked to tumor apoptosis. These reports indicated that delayed ROS release from mitochondria plays an important role in cytotoxicity of tumor cells exposed to genotoxic stimuli. Regarding the mechanism underlying DNA damage-induced increase in ROS release from the mitochondria, simultaneous increases in the intracellular ROS levels and mitochondrial contents have been closely linked in the cells of G2/M phase, which are arrested during the DNA damage checkpoint [21]. Because intracellular mitochondrial content increases in the order of G1, S, and G2/M phase [22] and the main source of intracellular ROS are believed to be the complexes I and III of ETC [23,24], intracellular ROS level is considered to be strongly dependent on mitochondrial content, which is regulated by the cell cycle. In addition, Yoshida *et al*. showed that γ-ray irradiation induces mtDNA damage and reduces NADH dehydrogenase activity, which is the most important enzyme that regulates ROS release from mitochondrial ETC [25]. However, there is not enough information concerning the redox status of mitochondrial ETC of tumor cells exposed to genotoxic stimuli, although this is important to understand the mechanism of delayed ROS release from the mitochondria.

Electron spin resonance (ESR) spectroscopy is widely utilized to evaluate mitochondrial redox status such as semiquinone (SQ) and iron–sulfur (Fe–S) cluster in various oxidative stress-related diseases, i.e., ischemia–reperfusion in cardiac muscles

[26], cardiomyopathy [27], sepsis [28], and tumor [29]. Ruuge *et al*. demonstrated that ischemia–reperfusion induces an increase in ESR signal intensities of SQ (g = 2.004) and Fe–S cluster of succinate dehydrogenase (g = 2.02) in isolated perfused hearts [26] and that mitochondria isolated from ischemic–reperfused hearts exhibit significant superoxide ($O_2^{\cdot -}$) capability than those from control hearts [30]. Burlaka *et al*. showed that the intensity of the ESR signal for SQ increases significantly and is dependent on the stage of gastric cancer, whereas that of Fe–S cluster (g = 1.94) in NADH dehydrogenase decreases. Furthermore, spin trap experiments using 1-hydroxy-2,2,6,6-tetramethyl-4-oxo-piperidine (TEMPONE-H) and Fe/DETC revealed that the production of $O_2^{\cdot -}$ and nitric oxide (NO) in tumor tissues increases with the stage of the disease [29]. From these experiments, ESR spectroscopy for cells and tissues can be used as a powerful tool to investigate the imbalance in mitochondrial redox status associated with energy production and ROS leakage from mitochondria during oxidative stress.

In this study, to elucidate the role of mitochondrial function in tumor cells exposed to X-rays, oxygen consumption ratio (OCR) and levels of mitochondrial ROS, F2-isoprostane (as a marker of oxidative damage), and adenosine nucleotides (as an indicator of intracellular energy status) were evaluated in X-irradiated HeLa cells. Furthermore, for evaluation of the redox status, levels of mitochondrial SQ and Fe–S cluster were also examined by low-temperature ESR measurements (103 K and 20 K).

Materials and Methods

Reagents

ATP, ADP, and AMP were obtained from Sigma-Aldrich (St. Louis, MO, USA). NAD^+ and NADH were obtained from Nacalai Tesque (Kyoto, Japan). MitoSOX Red was purchased from Thermo Fisher Scientific (Carlsbad, CA, USA). Tetra butyl ammonium

hydroxide was obtained from Wako Pure Chemical Co. (Osaka, Japan). 8-Iso $PGF_{2\alpha}$, 8-iso $PGF_{2\alpha}$-d4, 5-$iPF_{2\alpha}$-VI, and 5-$iPF_{2\alpha}$-VI-d11 were obtained from Cayman Chemicals (Ann Arbor, MI, USA).

Cell culture and treatment

Human cervical carcinoma HeLa cells were maintained in DMEM medium (Thermo Fisher Scientific, Waltham, MA, USA) supplemented with 10% fetal bovine serum at 37°C in 5% CO_2. X-Irradiation was performed using an X-Rad iR-225 (Precision X-Ray, North Branford, CT, USA). The dose rate was 1.37 Gy/min at 200 kVp, 15 mA, with a 1.0 mm aluminum filter. At indicated periods after 10 Gy of X-irradiation, cells were tripsinized and collected for further analysis.

Measurement of OCR by ESR spectroscopy

The peak-to-peak line width of the ESR spectrum of lithium 5,9,14,18,23,27,32,36-octa-n-butoxy-2,3-naphthalocyanine (LiNc-BuO) shows a liner response to partial pressure of oxygen (pO_2) [21]. LiNc-BuO was synthesized, according to the method described previously [31,32]. At indicated periods after 10 Gy of X-irradiation, cells were collected and washed three times with ice cold PBS. The cells were suspended in serum-free medium containing LiNc-BuO and 2% dextran to avoid sedimentation of the cells and LiNc-BuO. Thirty microliters of the cell suspension (1.25×10^7 cells/mL) was immediately drawn into a glass capillary tube, which was then sealed at both ends. ESR measurements were performed using a JEOL-RE X-band spectrometer (JEOL, Tokyo, Japan) with a cylindrical TE011 mode cavity (JEOL). The cavity was maintained at 37°C using a temperature controller (ES-DVT3; JEOL). The scanning parameters were as follows: 1 mW incident microwave power, 100 kHz modulation frequency, 6.3 μT field

modulation amplitude, and 5 mT scan range. The spectral line width was analyzed using a Win-Rad radical analyzer system (Radical Research, Tokyo, Japan). The ESR line width versus pO_2 calibration curve was constructed from ESR measurements based on LiNc-BuO equilibrated with oxygen/argon gas mixture.

Flow cytometric analysis of mitochondrial ROS levels in HeLa cells after X-irradiation

The fluorescent probe MitoSOX Red was used for assessing mitochondria-derived $O_2^{\cdot -}$. At 12 h after 10 Gy of X-irradiation, cells were collected and washed three times with ice cold PBS, then the cells were incubated in serum-free DMEM containing 2 μM MitoSOX Red for 30 min at 37°C. Then, the cells were trypsinized and washed twice with PBS. After re-suspending in PBS, the cells were analyzed using a BD FACSVerse flow cytometer (BD Biosciences, Franklin Lakes, NJ, USA). The mean MitoSOX Red fluorescence intensity of each sample was normalized to that of a control sample to calculate the relative MitoSOX Red intensity.

Measurement of cellular arachidonic acid oxidation products, F2-isoprostanes, by LC/MS/MS

At 12 or 24 h after 10 Gy of X-irradiation, cells were collected and washed three times with ice cold PBS, and resuspended in 300 μL of PBS in a 1.5-mL eppendorf tube. After 2 ng of deuterated internal standards were added to cell suspension, the cells were disrupted thrice by sonication (10 W; UR-20P, Tomy Seiko Co. Ltd, Tokyo, Japan) for 5 s. For measurement of F2-isoprostanes, the samples were subjected to solid phase extraction (SPE; NH_2 Sep-Pak cartridges, Waters Corporation, Milford, MA, USA), as described previously [33]. F2-isoprostanes in the aliquots were separated by Wakopak Ultra C18-3 (ϕ2.0 × 100 mm, 3 μm, Wako Pure Chemical Co.) at 45°C. The mobile phase

comprised two eluents: 0.15% NH_4OH (eluent A) and 95% acetonitrile, 5% MeOH, and 0.0125% NH_4OH (eluent B), and the flow rate was 0.35 mL/min. F2-isoprostanes were separated against a solvent gradient using 3% eluent B for 2 min followed by 30% of elute B for 8 min; separation was further achieved with 95% elute B for 5 min, and the solvent was maintained at 95% for 3 min. Column elute was directly coupled to a LCMS-8040 triple quadrupole mass spectrometer (Shimadzu, Kyoto, Japan) fitted with an electron spray ionization (ESI) operating in the negative ion mode. Multiple reaction monitoring (MRM) was used to analyze the various isoprostanes. 8-Iso $PGF_{2\alpha}$ was identified with a precursor-to-product ion transition *m/z* 353.4>193.1, 5-$iPF_{2\alpha}$-VI with transition *m/z* 353.4>115.1, 8-iso $PGF_{2\alpha}$-d4 with transition *m/z* 357.4>313.2, and 5-$iPF_{2\alpha}$-VI-d11 with transition *m/z* 364.3>115.15 (Supplementary Figure 1). Isoprostane concentrations were determined using their labeled internal standards. The extraction rates of 8-iso $PGF_{2\alpha}$, 5-$iPF_{2\alpha}$-VI, 8-iso $PGF_{2\alpha}$-d4, and 5-$iPF_{2\alpha}$-VI-d11 by SPE extraction procedures were approximately 77%, 77%, 77%, and 72%, respectively.

Measurement of cellular AMP, ADP, ATP, NAD^+, and NADH levels by LC/UV

Cellular AMP, ADP, ATP, NAD^+, and NADH levels were measured following the protocol published previously [34], with some modifications to the protocol. Briefly, at 12 or 24 h after 10 Gy of X-irradiation, the cells were collected and washed in manner similar to that described for the aforementioned LC/MS/MS experiments, 300 μL of 0.5 M KOH was added. The cells were lysed by passing through a 23-gauge needle 10 times. Cell lysate was neutralized by adding 120 μL of 10% phosphoric acid and centrifuged at 14,100 ×g for 30 min (4°C). The supernatant was separated by TSKgel ODS-80Ts (4.6 × 150 mm, 5 μm, Tosoh, Tokyo, Japan). The HPLC system (Tosoh) consisted of an autosampler (AS-8020), gradient pump (CCPM-II), and in-line degasser (SD-8022). The

mobile phase comprised two eluents: eluent A, 10 mM potassium phosphate (pH 5.0), 3% acetonitrile, and the ion pairing reagent tetra butyl ammonium hydroxide (TBAH; 2 mM); and eluent B, 10 mM potassium phosphate (pH 7.5) and 50% acetonitrile. The nucleotides were separated using a gradient starting at 100% eluent A for 0.6 min, then eluent B was increased to 25% for 1.5 min; eluent B was then further increased to 30% for 11.4 min, 70% for 3 min, and finally to 95% for 1.5 min. The flow rate was 0.8 mL/min, and detection was performed using a UV detector (UV-8020) at 260 nm. The concentration of cellular AMP, ADP, ATP, NAD^+, and NADH was calculated from the calibration curve and expressed as amount per 1×10^6 cells. Adenylate energy charge (AEC) was calculated according to the following formula:

$$AEC = \frac{[ATP] + 0.5[ADP]}{[ATP] + [ADP] + [AMP]} \qquad (1)$$

Measurement of the radicals derived from mitochondria by ESR

Cells (3×10^7) were trypsinized at 24 h after 10 Gy X-irradiation, collected by centrifugation at 1,000 rpm for 5 min (4°C), and washed twice with PBS. Next, cells were resuspended in 300 μL of PBS and transferred to natural quartz ESR tubes (ϕ5 mm × 250 mm, Tokyo Chemical Industry Co., Tokyo, Japan). For measurement at 103 K, ESR spectra were recorded using a JEOL-RE X-band spectrometer (JEOL) with a nitrogen temperature control system DVT-3 (JEOL). For measurement at 20 K, ESR spectra were recorded using ELEXSYS E580 (Bruker GmbH, Mannheim, Germany) with a helium temperature control system ER 4112HV (Bruker GmbH). The scanning parameters at 103 K and 20 K was as follows: 2 mW incident microwave power, 100 kHz modulation frequency, 1.0 mT field modulation amplitude, 50 mT scan range or 0.63 mT field modulation amplitude, and 5 mT scan range.

Statistical analysis

All results are expressed as mean ± standard error (SE) of at least three independent experiments. Statistical analyses were performed by Student's *t*-test. The minimum level of significance was set at $P < 0.05$.

Results

X-Irradiation enhances OCR and ROS production by mitochondria

Intracellular OCR is an important marker of mitochondrial energy metabolism because ETC in the mitochondria requires oxygen to produce ATP. Cellular OCR in non-irradiated and X-irradiated HeLa cells was measured by ESR oximetry using LiNc-BuO as the oxygen-sensitive probe. When non-irradiated cells were mixed with LiNc-BuO particles and ESR was performed at physiological temperature (37°C), the peak-to-peak line width of ESR spectrum decreased gradually in a time-dependent manner ("Control" in Figure 1A). Oxygen concentration calculated by the standard curve was plotted against incubation time (closed circles in Figure 1B), and the obtained OCR from the slope of this regression line was 6.0 ± 0.7 mmHg/1.25 × 10^5 cells. The presence of complex I inhibitor, rotenone, abolished the time-dependent decrease in the peak-to peak line width of ESR spectrum in non-irradiated HeLa cells ("Rotenone" in Figure 1A) and reduced the slope value to that of cell-free condition (open circles in Figure 1B), indicating that oxygen consumption was primarily due to mitochondrial oxygen metabolism. Furthermore, it was shown that the line width of the ESR spectrum ("X-irradiation" in Figure 1A) obtained from HeLa cells at 24 h after irradiation rapidly decreased compared to that ("Control" in Figure 1A) of the ESR spectrum of non-irradiated cells. In the OCR data summarized in Figure 1C, OCR of X-irradiated cells (8.7 ± 0.5 mmHg/1.25 × 10^5 cells) was significantly higher, by approximately 1.5-fold, than that of non-irradiated cells

(6.0 ± 0.7 mmHg/1.25 × 10^5 cells). In addition, rotenone inhibited the time-dependent decrease of peak-to peak line width of ESR spectrum in both non-irradiated and irradiated cells ("Rotenone" and "X-Irradiation + Rotenone" in Figure 1B) and there was no significant difference in the OCR between non-irradiated and irradiated cells in the presence of rotenone (Figure 1C). These observations indicated that X-irradiation induced an increase in mitochondrial oxygen metabolism, including ETC activity.

Because it has been reported that the release of ROS from mitochondria is due to $O_2^{\cdot -}$ produced by the reaction of oxygen with the electrons leaked from complexes I and III of ETC [23,24], there is a possibility that excess leakage of electrons from ETC, mediated by X-irradiation, enhances intracellular ROS level including that of $O_2^{\cdot -}$. To examine this possibility, intracellular ROS levels of X-irradiated HeLa cells were analyzed by flow cytometry with the $O_2^{\cdot -}$-sensitive fluorescent probe, MitoSOX Red. As shown in Figures 1D and E, cells collected 24 h after X-irradiation exhibited higher MitoSOX Red fluorescence intensity than that exhibited by non-irradiated cells. In addition, the treatment of rotenone increased MitoSOX Red fluorescence intensity compared to that observed in the non-irradiated cells, and further enhanced the MitoSOX Red fluorescence intensity of the irradiated cells. These results suggest that X-irradiation induces mitochondrial ROS production concomitantly with the activation of mitochondrial ETC.

Effects of X-irradiation on intracellular F2-isoprostane

Next, to evaluate the effect of X-irradiation-induced ROS production on intracellular lipid peroxidation levels, we analyzed F2-isoprostane levels, a lipid peroxidation product of arachidonic acid, by LC/MS/MS. Arachidonic acid is the predominant polyunsaturated fatty acid (PUFA) in mammalian cells and plays an important role in maintaining cell

membrane integrity. Isoprostanes are a series of prostaglandin-like compounds that are formed non-enzymatically *in vivo* via the peroxidation of arachidonic acid by a free radical-initiated mechanism [33]. We performed MRM to select the ion and have shown the precursor and predominant fragment ions of standard materials in supplementary Figures 1A (upper panel) and B (upper panel). Furthermore, the chromatograms of 8-iso $PGF_{2\alpha}$ and 5-$iPF_{2\alpha}$-VI are shown in supplementary Figures 1A (lower panel) and B (lower panel), respectively. The retention time of 8-iso $PGF_{2\alpha}$ and 5-$iPF_{2\alpha}$-VI was 7.8 min and 8.2 min, respectively, and the peaks of cell samples were determined from the retention times of standard samples. Supplementary Figure 1C shows the chromatograms of cellular 8-iso $PGF_{2\alpha}$ (upper panel) and deuterated internal standard 8-iso $PGF_{2\alpha}$-d4 (lower panel) from the non-irradiated cells, and supplementary Figure 1D shows the chromatograms of cellular 5-$iPF_{2\alpha}$-VI (upper panel) and deuterated internal standard 5-$iPF_{2\alpha}$-VI-d11 (lower panel) from the non-irradiated cells. Figure 2A shows the time course of 8-iso $PGF_{2\alpha}$ contents after X-irradiation. 8-Iso $PGF_{2\alpha}$ contents remained unaltered until 24 h after X-irradiation. Figure 2B shows the time course of 5-$iPF_{2\alpha}$-VI contents after X-irradiation. 5-$iPF_{2\alpha}$-VI contents also remained unaltered until 24 h after X-irradiation. Figure 2C shows the quantitative values of intracellular 8-iso $PGF_{2\alpha}$ from area values. 8-iso $PGF_{2\alpha}$ level in the cells at 24 h after X-irradiation did not increase significantly compared with that in non-irradiated cells. However, 8-Iso $PGF_{2\alpha}$ level increased significantly in cells treated with rotenone compared with that in non-treated cells. Similar tendencies were also observed for 5-$iPF_{2\alpha}$-VI (Figure 2D). These results indicate that X-irradiation-induced increase in intracellular ROS level was not enough to significantly increase membrane oxidative damage.

Cellular homeostasis is maintained after X-irradiation

Next, to evaluate whether X-irradiation-induced activation of mitochondrial ETC impacts cellular energy metabolism, intracellular AMP, ADP, ATP, NAD^+, and NADH levels were measured by LC/UV. A typical chromatogram (control) obtained from HeLa cells without X-irradiation is shown in the upper panel of Figure 3A. The retention times were 6.1 min, 11.4 min, 16.9 min, 21.0 min, and 23.3 min in the elution profile of NAD^+, AMP, NADH, ADP, and ATP, respectively, by comparison with retention times of control substances. In HeLa cells at 24 h after X-irradiation, the elution profile (bottom panel of Figure 3A) revealed that the peak height of AMP, ADP, and ATP apparently increased in comparison with that of non-irradiated control. The time course of intracellular AMP, ADP, ATP, NAD^+, and NADH in HeLa cells after X-irradiation is denoted in Figures 3B and C. Intracellular concentration of ATP started to increase at 12 h after irradiation and that of ATP, ADP, and AMP significantly increased at 24 h after irradiation, although the values of AEC in HeLa cells at 12 and 24 h after irradiation were maintained at levels of the non-irradiated control. Next, to elucidate the involvement of mitochondrial F_0F_1-ATPase/ATP synthase on radiation-induced increase in ATP levels, cells were incubated with 2 ng/mL oligomycin for 12 h after irradiation. As shown in Figure 3C, treatment with oligomycin did not influence the basal ATP level of non-irradiated cells; however, this treatment completely abolished a portion of X-irradiation-induced increase in intracellular ATP levels. Intracellular concentration of NAD^+ significantly increased at 12 h after irradiation, and there were no significant changes in the intracellular concentration of NADH. However, the NAD^+-to-NADH ratio (NAD^+/NADH) remained unchanged until 24 h after X-irradiation, although an increasing tendency was observed (Figure 3D). These data suggest that production of intracellular F_0F_1-ATPase/ATP synthase-dependent ATP with increase in NAD^+ levels is a response to irradiation.

X-Irradiation increases ESR signal intensity at g = 2.004 in HeLa cells

Increase in rotenone-sensitive OCR and levels of oligomycin-sensitive ATP on X-irradiation of HeLa cells (Figure 1A–C and Figure 3C) suggests that X-irradiation activates mitochondrial functions. To analyze the mitochondrial ETC system after irradiation, ESR was performed for whole cells. When the ESR spectrum of 3×10^7 HeLa cells was recorded at 103 K, two distinct signals at g = 1.941 and g = 2.004 were primarily observed (Figure 4A, upper panel). In previous ESR studies [35], it has been reported that most normal tissues and their isolated cells yield similar ESR spectra, with prominent peaks at g = 2.004 and g = 1.94. As shown in supplemental Figure 2, two peaks at g = 2.004 and g = 1.941 in heart tissue, liver tissue from mouse, and isolated mitochondria from bovine heart were also observed in our experimental condition. Similar ESR signals have been reported in many tumor cells, such as human cervical carcinoma HeLa cells [36], lung adenocarcinoma A549 cells [37], and several gastric tumor cells (T2-4, N0-2, M0-1, and G1-G4 cells) [29]. Emanuel reported that a narrow ESR signal at g = 2.004 is due to radicals of SQ, which are primarily localized in the mitochondria, and the broader signal at g = 1.94 originates from the non-heme iron of mitochondria containing sulfur compounds in various types of cancer [38].

Previous reports have shown that saturation of the g = 2.004 signal in mitochondrial SQ of *E. coli* [39] and bovine heart mitochondrial SQ at 77 K [40] occurred at a very low microwave power level (<10 μW), with the power for half saturation ($P_{1/2}$) being 10–100 μW. For the g = 1.94 signal of ferredoxin-type Fe–S cluster (2Fe–2S) at a temperature of 12.5–20.7 K for various plant, bacterial, and adrenal mitochondria, the values of $P_{1/2}$ were reported to be ranged from ≤0.1 mW to 0.4 mW [41]. These observations indicate that the relaxation time of Fe–S clusters is relatively short compared to that of SQ radicals. In fact, as shown in supplementary Figure 3, the value of $P_{1/2}$ of g

= 2.004 signal was 40 μW at 103 K, and that of $P_{1/2}$ of g = 1.941 at 103 K and 20 K was 0.35 mW and 0.22 mW, respectively. These observations indicate that g = 2.004 and g = 1.941 signals observed in whole mammalian cells (Figure 4A, upper panel) originate from mitochondrial SQ radical and mitochondrial ferredoxin-type Fe–S cluster, respectively.

Next, HeLa cells were irradiated with 10 Gy of X-rays, incubated for 24 h, and the ESR spectrum of 3×10^7 whole cells were obtained at 103 K (Figure 4A, lower panel). When the peak height of each ESR signal was measured, it was demonstrated that the intensity of ESR signal at g = 2.004 was significantly enhanced as shown in Figure 4C. Jong and Albracht [40] and Vinogradov *et al*. [42,43] demonstrated that activation of the respiratory chain in bovine heart submitochondrial particles by NADH or succinate enhances the intensity of ESR signal at g = 2.004 and that rotenone abolishes this response, indicating that SQ radicals act as obligatory intermediates of ETC in the mitochondria. To clarify the relationship between radiation-induced enhancement of ESR signal at g = 2.004 and mitochondrial functions, HeLa cells were incubated in the presence of a complex I inhibitor, rotenone, in mitochondrial ETC systems after X-irradiation. X-irradiation-induced increase in response of g = 2.004 signal was completely abolished by incubation with rotenone (Figure 4B). In non-irradiated HeLa cells, quantitative analysis revealed that the ESR signal intensity at g = 2.004 was attenuated to about half by incubation with rotenone, indicating that the g = 2.004 signal was partly derived from complex I. Furthermore, it was shown that the intensity of the g = 2.004 signal obtained from X-irradiated HeLa cells with rotenone was quite similar to that of non-irradiated HeLa cells with rotenone (Figure 4C). These data indicated that X-irradiation-enhanced SQ was strongly associated with mitochondrial ETC systems.

In contrast, the intensity of ESR signals at g = 1.941 seemed to be not influenced by X-irradiation as shown in Figure 4A. However, the quantitative measurement of the

ESR signal at g = 1.941 may be not accurate because the line width (7.5 mT) of this ESR signal was too broad due to very short relaxation time at approximately 103 K. To obtain more accurate data, the ESR spectra of HeLa cells without or with X-irradiation were measured at 20 K. It was observed that the line width of ESR signals at g = 1.941 at 20 K was 4.1 mT, and this ESR signal with high signal-to-noise ratio was suitable for quantitative analysis (Figure 5A, upper panel). Moreover, it was clearly demonstrated that the intensity of the ESR signal at g = 1.941 was not influenced by X-irradiation (Figure 5B). These phenomena suggest that X-irradiation enhances SQ radicals but not Fe–S cluster.

Discussion

Recent studies have demonstrated that exposure to radiation in human colorectal carcinoma cell line HCT116, osteosarcoma cell line HPS11 [44], and human lung cell carcinoma A549 [21] leads to the activation of mitochondrial energy metabolism and mitochondrial ATP production. These reports suggested that the cellular switch mechanism of energy metabolism in mitochondrial respiration provides additional advantage for cell survival because several lipophilic triphenylphosphonium derivatives enhance radiation-induced cell death via inhibition of mitochondrial energy metabolism [7]. The present study also showed that radiation-induced increases in the rotenone-sensitive OCR (Figures 1B and C) and oligomycin-sensitive ATP levels (Figure 3C) were observed at 24 h after X-irradiation, whereas AEC values after X-irradiation were stable (0.76–0.86). Extensive biochemical studies have shown that the narrow margin (between 0.7 and 0.95) of AEC values is preserved at physiological conditions in a wide variety of eukaryotes and prokaryotes [45,46], and this value decreases during the pathological conditions that lead to reduced energy levels, such as rotenone treatment [47], hypoxia

[48,49], and ischemic condition [50]. Moreover, after X-irradiation, NADH level was not altered and NAD^+ and ATP levels increased drastically, suggesting that there is ample supply of NADH from the tricarboxylic acid (TCA) cycle or other routes after X-irradiation. These results may indicate that radiation-induced increase in cellular NAD^+ and ATP pool is operated under physiological homeostasis. Moreover, this radiation-induced increase in cellular NAD^+ and ATP pool (Figure 3) may act as an adaptive or protective response against DNA damage after genotoxic stimuli, because decrease in NAD^+ and ATP levels triggered by poly(ADP-ribose) polymerase 1 (PARP1)-driven-metabolic catastrophe has been reported to enhance radiation-induced programmed-necrosis in human prostate NQO1 cancer positive cells (PC-3, DU145, and LNCaP) exposed to β-lapachone [a substrate of NADH:quinone oxidoreductase 1 (NQO1)] [51]. This likely indicates that the mitochondrial ETC system related to radiation-induced increase in NAD^+ and ATP pool is an important target for radiosensitization in cancer radiation therapy.

Recently, numerous DNA damaging agents, including X-irradiation and anticancer drugs, have been reported to induce increase in mitochondrial ROS levels as a late event in various cell lines [10-20], and this production of ROS is associated with apoptosis [52] and senescence [53]. As shown in Figures 1D, 1E, and 2, the marginal increase in radiation-induced response of mitochondrial ROS was confirmed in HeLa cells, although lipid peroxides, such as 5-i$PF_{2\alpha}$-VI and 8-iso$PGF_{2\alpha}$ were not influenced until 24 h after X-irradiation. As shown in Figure 1E, inhibition of mitochondrial respiratory chain complex I by rotenone elevated basal level of mitochondrial ROS production and X-irradiation induced further increase of ROS production in the presence of rotenone. This observation suggested that ROS was originated from Complex I, and X-irradiation facilitated electron flow to complex I in ETC and the overflowed electron

reacted with molecular oxygen, resulting in X-irradiation-induced increase of ROS production in Complex I. In Figures 2C and 2D, the production of 8-isoPGF$_{2\alpha}$ and 5-iPF$_{2\alpha}$-VI stayed similar level between untreated and X-irradiated cells, although there was a significant difference in their production when the cells were treated with rotenone. This observation may be explained by the existence of qualitative limitations of cellular intrinsic antioxidants, i.e., vitamin E, ascorbate, GSH, SOD and catalase, against oxidative stress. In other words, these phenomena suggested that cellular antioxidants were enough existed to prevent cellular oxidative damages when the concentration of cellular ROS is relatively lower level in the cells X-irradiated without rotenone. Whereas cellular oxidative damages such as lipid peroxide might be significantly accumulated by the reaction of biomolecules with ROS that could not be detoxicated by the intrinsic antioxidants when the concentration of ROS is high level in the cells X-irradiated with rotenone.

In radiation response in glycolysis in tumor cells, Fujibayashi *et al*., demonstrated that the upregulation of glycolysis-associated gene products (glucose transporter protein type 1 [SLC2A1] and hexokinase) and increase of uptake of [^{3}H]-2-deoxy-D-glucose in human colon adenocarcinoma LS180 cells occurred at 3 - 5 h after 30 Gy of X-irradiation [54]. This radiation-induced increase of uptake of [^{3}H]-2-deoxy-D-glucose was shown to be completely diminished by the inhibitors of both mRNA (actinomycin D) and protein synthesis (cycloheximide), indicating that the transiently elevated glucose metabolism occurred via processes at the levels of gene expression. Recently, in human hepatoma HepG2 cells and striated muscle HMCL-7304 cells, Wang *et al*., have reported a concomitant elevation of glucose 6-phosphate and the two pyruvate metabolites lactate and alanine at 4 h after 2 Gy of γ-irradiation, suggesting induction of enhancement of cytosolic aerobic glycolysis by X-irradiation [55]. In our preliminary experiment (data

not shown), we confirmed the increase of lactate concentration in the medium as a marker of aerobic glycolysis at 24 h after exposure of 10 Gy X-rays to HeLa cells, suggesting that X-irradiation also increase mitochondrial ETC but also aerobic glycolysis in our present condition. However, as shown in Figure 3C, oligomycin completely abolished X-irradiation-induced increase in ATP, meaning that X-irradiation-induced increase of ATP was mainly derived from mitochondrial F_0F_1-ATPase/ATP synthase in complex IV but not aerobic glycolysis. From these data, it could be inferred that X-irradiation-induced increase of aerobic glycolysis did not significantly contribute to total ATP production in HeLa cells, because efficiency of ATP production (2 ATP per a glucose molecule) in glycolysis was considerably smaller than that (36 ATP per a glucose molecule) in oxidative phosphorylation.

Because the main source of mitochondrial ROS was believed to be leakage of electrons from complexes I and III [23,24], effects of X-irradiation on SQ and Fe–S cluster, which play a crucial role in these complexes of mitochondrial ETC, were evaluated by ESR under low temperature. Based on the results of power saturation experiments (Supplementary Figure 3) and rotenone treatment (Figure 4) in non-irradiated HeLa cells, g = 2.004 and g = 1.941 signals were identified as SQ and mitochondrial ferredoxin-type Fe–S clusters, respectively. Moreover, it was demonstrated that X-irradiation enhanced the signal intensity of SQ but not Fe–S clusters. Furthermore, it was clearly demonstrated that rotenone treatment reduced basal intensity of SQ signals and abolished the increase in SQ signal induced by X-irradiation (Figure 4). De Jong and Albracht [40] and Burbaev *et al.* [42] reported that the short time reaction (10 millisecond–15 s) of NADH with submitochondrial particles isolated from bovine heart enhances the signal intensity of SQ at g = 2.004 but not Fe–S cluster at g = 1.94 and this NADH-induced enhancement of SQ signal is abolished with rotenone treatment,

indicating that SQ form obligatory intermediates in the reaction of complex I with ubiquinone. From these reports, our observation suggests the enhancement of electron flow in rotenone-sensitive ETC in the mitochondria 24 h after X-irradiation. However, the signal intensity of Fe–S cluster was not influenced by X-irradiation, although other oxidative stress such as ischemia [56] and cardiomyopathy in mouse heart [27], alter the signal intensity of Fe–S cluster by oxidation of the iron ion in Fe–S clusters. Burlaka *et al*. showed that exposure to electromagnetic radiation of ultra-high frequency in rats decreased the ESR intensity at the g = 2.00 and g = 1.94 signals in liver, cardiac, and aorta tissues [57].

Our previous studies have demonstrated that mitochondria mass, mitochondrial DNA (D-loop and cytochrome c oxidase subunit II [COXII] in A549 cells [21], and NADH dehydrogenase subunit 6 [DN6] in NIH3T3 cells [6]), the expression of PPARγ coactivator-1α (α mitochondrial biogenesis-related gene) in NIH3T3 cells were enhanced by X-irradiation, although X-irradiation hardly influenced the expression of two mitochondrial proteins, cytochrome c oxidase subunit IV and cytochrome c [6]. As shown in Figure 4A and 5, the ESR data suggested the X-irradiation induced increase in electron flow in complex I-related SQ but did not unchanged amount of Fe-S cluster. Though the aerobic glycolysis (Warburg effect) seems to be enhanced by X-irradiation, cellular NADH as an electron donor for the mitochondrial ETC was not altered until 24 h after X-irradiation as shown in Figure 3D. Taken together, X-irradiation induces increase of mitochondrial mass and/or an imbalance of expression of some components related with ETC, thereby increasing reaction of oxygen with the electrons leaked from ETC to produce $O_2^{\cdot -}$. To clarify the precise mechanism for late production of ROS and increase of ATP after exposure of X-rays to tumor cells, further experiments to examine

the radiation-induced response in energy metabolism of not only ETC but also glycolysis, glutaminolysis and TCA cycle are necessary in the next step.

In summary, the present study clearly demonstrated that X-irradiation induced an increase in OCR, ATP levels, and leakage of ROS at 24 h after X-irradiation, indicating the activation of mitochondrial function. During this mitochondrial activation, the values of AEC and NADH were maintained within the range of physiological condition. However, X-irradiation induced an increase in SQ radical levels but not in Fe–S cluster levels, suggesting redox imbalance in the mitochondria of X-irradiated cells. These results suggested that the leakage of excess electrons triggered by this mitochondrial redox imbalance reacted with molecular oxygen, leading to an increase in intracellular $O_2^{\cdot -}$ levels. In addition, the combined application of ESR oximetry and low-temperature ESR spectroscopy to analyze whole cells showed that this combination is a powerful tool for analyzing the mitochondrial redox status.

Acknowledgements

We would also like to thank Editage (www.editage.jp) for English language editing.

Disclosure statement

The authors report no conflicts of interest. The authors alone are responsible for the content and writing of this article.

Funding

This work was supported, in part, by Grant-in-Aids for Scientific Research from Japan Society for the Promotion of Science [grant Numbers 26461875, 17K10465 (TY),

17H03920 (OI)]. The sponsors had no role in the study design; in the collection, analysis, and interpretation of data; in the writing of the manuscript; nor the decision to submit the manuscript for publication.

References

[1] Warburg O. On the origin of cancer cells. Science 1956;123(3191):309-14.

[2] Zeng WX, Rabinowitz JD, White E. Mitochondria and Cancer. Mol Cell 2016;61(5):667-76.

[3] Chen Y, McMillan-Ward E, Kong J, et al. Mitochondrial electron-transport-chain inhibitors of complexes I and II induce autophagic cell death mediated by reactive oxygen species. J Cell Sci 2007;120(Pt 23):4155-66.

[4] Lu CL, Qin L, Liu HC, et al. Tumor cells switch to mitochondrial oxidative phosphorylation under radiation via mTOR-mediated hexokinase II inhibition-a Warburg-reversing effect. PLoS One 2015;10(3):e0121046.

[5] Yamamori T, Ike S, Bo T, et al. Inhibition of the mitochondrial fission protein dynamin-related protein 1 (Drp1) impairs mitochondrial fission and mitotic catastrophe after x-irradiation. Mol Biol Cell 2015;26(25):4607-17.

[6] Yamamori T, Sasagawa T, Ichii O, et al. Analysis of the mechanism of radiation-induced upregulation of mitochondrial abundance in mouse fibroblasts. J Radiat Res 2017;58(3):292-301.

[7] Yasui H, Yamamoto K, Suzuki M, et al. Lipophilic triphenylphosphonium derivatives enhance radiation-induced cell killing via inhibition of mitochondrial energy metabolism in tumor cells. Cancer Lett 2017;390:160-167.

[8] Marrache S, Pathak RK, Dhar S. Detouring of cisplatin to access mitochondrial genome for overcoming resistance. Proc Natl Acad Sci U S A 2014;111(29):10444-9.

[9] Nishida N, Yasui H, Nagane M, et al. 3-Methyl pyruvate enhances radiosensitivity through increasing mitochondria-derived reactive oxygen species in tumor cell lines. J Radiat Res 2014;55(3):455-63.

[10] Indo HP, Inanami O, Koumura T, et al. Roles of mitochondria-generated reactive oxygen species on X-ray-induced apoptosis in a human hepatocellular carcinoma cell line, HLE. Free Radic Res 2012;46(8):1029-43.

[11] Motoori S, Majima HJ, Ebara M, et al. Overexpression of mitochondrial manganese superoxide dismutase protects against radiation-induced cell death in the human hepatocellular carcinoma cell line HLE. Cancer Res 2001;61(14):5382-8.

[12] Chen Z, Wang B, Yu F, et al. The roles of mitochondria in radiation-induced autophagic cell death in cervical cancer cells. Tumor Biol 2016;37(3):4083-91.

[13] Hosoki A, Yonekura S, Zhao QL, et al. Mitochondria-targeted superoxide dismutase (SOD2) regulates radiation resistance and radiation stress response in HeLa cells. J Radiat Res 2012;53(1):58-71.

[14] Hu S, Gao Y, Zhou H, et al. New insight into mitochondrial changes in vascular endothelial cells irradiated by gamma ray. Int J Radiat Biol 2017;93(5):470-476.

[15] Fetisova EK, Antoschina MM, Cherepanynets VD, et al. Radioprotective effects of mitochondria-targeted antioxidant SkQR1. Radiat Res 2015;183(1):64-71.

[16] Saenko Y, Cieslar-Pobuda A, Skonieczna M, et al. Changes of reactive oxygen and nitrogen species and mitochondrial functioning in human K562 and HL60 cells exposed to ionizing radiation. Radiat Res 2013;180(4):360-6.

[17] Kobashigawa S, Kashino G, Suzuki K, et al. Ionizing radiation-induced cell death is partly caused by increase of mitochondrial reactive oxygen species in normal human fibroblast cells. Radiat Res 2015;183(4):455-64.

[18] Kashino G, Tamari Y, Kumagai J, et al. Suppressive effect of ascorbic acid on the mutagenesis induced by the bystander effect through mitochondrial function. Free Radic Res 2013;47(6-7):474-9.

[19] Choi YM, Kim HK, Shim W, et al. Mechanism of Cisplatin-Induced Cytotoxicity Is Correlated to Impaired Metabolism Due to Mitochondrial ROS Generation. PLoS One 2015;10(8):e0135083.

[20] Sorokina IV, Denisenko TV, Imreh G, et al. Reactive oxygen species regulate a balance between mitotic catastrophe and apoptosis. Int J Biochem Cell Biol 2016;81(Pt A):133-136.

[21] Yamamori T, Yasui H, Yamazumi M, et al. Ionizing radiation induces mitochondrial reactive oxygen species production accompanied by upregulation of mitochondrial electron transport chain function and mitochondrial content under control of the cell cycle checkpoint. Free Radic Biol Med 2012;53(2):260-70.

[22] Jahnke VE, Sabido O, Freyssenet D. Control of mitochondrial biogenesis, ROS level, and cytosolic Ca^{2+} concentration during the cell cycle and the onset of differentiation in L6E9 myoblasts. Am J Physiol Cell Physiol 2009;296(5):C1185-94.

[23] Schonfeld P, Wojtczak L. Fatty acids decrease mitochondrial generation of reactive oxygen species at the reverse electron transport but increase it at the forward transport. Biochim Biophys Acta 2007;1767(8):1032-40.

[24] Lanciano P, Khalfaoui-Hassani B, Selamoglu N, et al. Molecular mechanisms of superoxide production by complex III: a bacterial versus human mitochondrial comparative case study. Biochim Biophys Acta 2013;1827(11-12):1332-9.

[25] Yoshida T, Goto S, Kawakatsu M, et al. Mitochondrial dysfunction, a probable cause of persistent oxidative stress after exposure to ionizing radiation. Free Radic Res 2012;46(2):147-53.

[26] Ruuge EK, Ledenev AN, Lakomkin VL, et al. Free radical metabolites in

myocardium during ischemia and reperfusion. Am J Physiol 1991;261(4 Suppl):81-6.

[27] Elas M, Bielanska J, Pustelny K, et al. Detection of mitochondrial dysfunction by EPR technique in mouse model of dilated cardiomyopathy. Free Radic Biol Med 2008;45(3):321-8.

[28] Svistunenko DA, Davies N, Brealey D, et al. Mitochondrial dysfunction in patients with severe sepsis: an EPR interrogation of individual respiratory chain components. Biochim Biophys Acta 2006;1757(4):262-72.

[29] Burlaka AP, Ganusevich, II, Gafurov MR, et al. Stomach Cancer: Interconnection between the Redox State, Activity of MMP-2, MMP-9 and Stage of Tumor Growth. Cancer Microenviron 2016;9(1):27-32.

[30] Ledenev AN, Ruuge EK. Generation of superoxide radicals by mitochondria of the ischemic heart. Bull. Exp. Biol. Med. 1985;100(3):1204-1206.

[31] Pandian RP, Parinandi NL, Ilangovan G, et al. Novel particulate spin probe for targeted determination of oxygen in cells and tissues. Free Radic Biol Med 2003;35(9):1138-48.

[32] Fujii H, Sakata K, Katsumata Y, et al. Tissue oxygenation in a murine SCC VII tumor after X-ray irradiation as determined by EPR spectroscopy. Radiother Oncol 2008;86(3):354-60.

[33] Labuschagne CF, van den Broek NJ, Postma P, et al. A protocol for quantifying lipid peroxidation in cellular systems by F2-isoprostane analysis. PLoS One 2013;8(11):e80935.

[34] Bornhorst J, Ebert F, Lohren H, et al. Effects of manganese and arsenic species on the level of energy related nucleotides in human cells. Metallomics 2012;4(3):297-306.

[35] Swartz HM. Biological Applications of Electron Spin Resonance. Hoboken: John Wiley & Sons Inc; 1972. Chapter 4, Cells and Tissues; p. 155-196.

[36] Segre AL, Benedetto A, Eremenko T, et al. An electron paramagnetic resonance study of free radicals in cells. Biochim Biophys Acta 1977;497(2):615-21.

[37] Jakubowska M, Sniegocka M, Podgorska E, et al. Pulmonary metastases of the A549-derived lung adenocarcinoma tumors growing in nude mice. A multiple case study. Acta Biochim Pol 2013;60(3):323-30.

[38] Emanuel NM. Kinetics and the free-radical mechanisms of tumor growth. Ann N Y Acad Sci 1973;222:1010-30.

[39] Swartz HM. Effect of oxygen on freezing damage: II. Physicalchemical effects. Cryobiology 1971;8(3):255-264.

[40] De Jong AM, Albracht SP. Ubisemiquinones as obligatory intermediates in the electron transfer from NADH to ubiquinone. Eur J Biochem 1994;222(3):975-82.

[41] Rupp H, Rao KK, Hall DO, et al. Electron spin relaxation of iron-sulphur proteins studied by microwave power saturation. Biochim Biophys Acta 1978;537(2):255-269.

[42] Burbaev DS, Moroz IA, Kotlyar AB, et al. Ubisemiquinone in the NADH-ubiquinone reductase region of the mitochondrial respiratory chain. FEBS Letters 1989;254(1):47-51.

[43] Kotlyar AB, Sled VD, Burbaev DS, et al. Coupling site I and the rotenone-sensitive ubisemiquinone in tightly coupled submitochondrial particles. FEBS Letters 1990;264(1):17-20.

[44] Bartoletti-Stella A, Mariani E, Kurelac I, et al. Gamma rays induce a p53-independent mitochondrial biogenesis that is counter-regulated by HIF1alpha. Cell Death Dis 2013;4:e663.

[45] Derr RF, Zieve L. Adenylate energy charge: relation to guanylate energy charge and the adenylate kinase equilibrium constant. Biochem Biophys Res Commun 1972;49(6):1385-90.

[46] Privalle LS, Burris RH. Adenine nucleotide levels in and nitrogen fixation by the cyanobacterium Anabaena sp. strain 7120. J Bacteriol 1983;154(1):351-5.

[47] Matsumoto SS, Raivio KO, Seegmiller JE. Adenine nucleotide degradation during energy depletion in human lymphoblasts. Adenosine accumulation and adenylate energy charge correlation. J Biol Chem 1979;254(18):8956-62.

[48] Danielsen T, Skoyum R, Rofstad EK. Hypoxia-induced changes in radiation sensitivity in human melanoma cells: importance of oxygen-regulated proteins, adenylate energy charge and cell cycle distribution. Radiother Oncol 1997;44(2):177-82.

[49] Skoyum R, Eide K, Berg K, et al. Energy metabolism in human melanoma cells under hypoxic and acidic conditions in vitro. Br J Cancer 1997;76(4):421-8.

[50] Balestri F, Giannecchini M, Sgarrella F, et al. Purine and pyrimidine nucleosides preserve human astrocytoma cell adenylate energy charge under ischemic conditions. Neurochem Int 2007;50(3):517-23.

[51] Dong Y, Bey EA, Li LS, et al. Prostate cancer radiosensitization through poly(ADP-Ribose) polymerase-1 hyperactivation. Cancer Res 2010;70(20):8088-96.

[52] Ogura A, Oowada S, Kon Y, et al. Redox regulation in radiation-induced cytochrome c release from mitochondria of human lung carcinoma A549 cells. Cancer Lett 2009;277(1):64-71.

[53] Passos JF, Nelson G, Wang C, et al. Feedback between p21 and reactive oxygen production is necessary for cell senescence. Mol Syst Biol 2010;6:347.

[54] Fujibayashi Y, Waki A, Sakahara H, et al. Transient increase in glycolytic metabolismin cultured tumor cells immediately after exposure to ionizing radiation:From gene expressionto deoxyglucose uptake. Radiat. Res. 1997;147:729-34.

[55] Wang M. Keogh A, Treves S., et al. The metabolomic profile of gamma-irradiated human hepatoma and muscle cells reveals metabolic changes consistent with the Warburg effect. Peer J 4:e1624; DOI 10.7717/peerj.1624

[56] Baker JE, Kalyanaraman B. Ischemia-induced changes in myocardial paramagnetic metabolites: implications for intracellular oxy-radical generation. FEBS Lett 1989;244(2):311-4.

[57] Burlaka A, Selyuk M, Gafurov M, et al. Changes in mitochondrial functioning with electromagnetic radiation of ultra high frequency as revealed by electron paramagnetic resonance methods. Int J Radiat Biol 2014;90(5):357-62.

Figure legends

Figure 1. Oxygen consumption rate (OCR) and mitochondrial reactive oxygen species (ROS) levels in HeLa cells after 10 Gy of X-irradiation without and with 10 μM of rotenone. (A) Representative time-course of ESR spectra of the extracellular oxygen probe LiNc-BuO in the presence of cells at 37°C without X-irradiation and rotenone (Control), with X-irradiation (X-Irradiation), with rotenone (Rotenone) and with X-irradiation and rotenone (X-Irradiation + Rotenone). After irradiation, cells were incubated for 24 h, cells (1.25×10^7 cells/mL) were collected, and re-suspended in ice-cold medium containing LiNc-BuO and 2% dextran in an air-tight glass capillary tube. ESR spectra were measured from 1.5 to 31.5 min (at intervals of 3 min) after heating up to 37°C. Two-faced arrow indicates line widths of ESR signal at 1.5 min. (B) Time-dependent changes in pO_2 (mmHg/1.25×10^5 cells) calculated from ESR line width of LiNc-BuO in HeLa cells at 37°C without (●, Control) and with 10 Gy of X-irradiation (■, X-Irradiation). Calibration curve of line-width against pO_2 as described in our previous report [21] was used for determining extracellular pO_2. In case of rotenone treatments, rotenone (final concentration 10 μM) was added to the cell suspension just before ESR measurement. ○, 10 μM rotenone; □, combination of X-irradiation and rotenone. (C) OCR (mmHg/min·1.25×10^5 cells) of HeLa cells was calculated by regression curves of (B). Data are expressed as means ± SE of three experiments. *$P < 0.05$, **$P < 0.01$ (Student's *t*-test). (D) Mitochondrial ROS levels were measured by flow cytometry using MitoSOX Red. Representative flow cytometric profiles were obtained from the cells at 0 (control) and 24 h (X-rays) after X-irradiation. (E) Summarized data of the relative mitochondrial ROS levels without and with 10 Gy

of X-irradiation. In case of rotenone treatments, rotenone (final concentration 1 μM) was added to the medium immediately after irradiation and cells were incubated for 12 h. Data are expressed as means ± SE of three experiments. $^{**}P < 0.01$ (Student's *t*-test).

Figure 2. LC/MS/MS measurements of cellular F2-isoprostane in HeLa cells after X-irradiation. Time-dependent changes in the amount of 8-iso $PGF_{2\alpha}$ (A) and 5-$iPF_{2\alpha}$-VI (B) in HeLa cells after irradiation were evaluated by LC/MS/MS with ESI. Effect of rotenone on cellular 8-iso $PGF_{2\alpha}$ (C) and 5-$iPF_{2\alpha}$-VI levels (D) in non-irradiated and irradiated HeLa cells at 24 h was evaluated by LC/MS/MS analysis. Treatments with rotenone are similar to those described in Figure 1E. Data are expressed as means ± SE of three experiments. $^{*}P < 0.05$, $^{**}P < 0.01$ (Student's *t*-test).

Figure 3. Cellular AMP, ADP, ATP, NAD^+, and NADH levels in HeLa cells after X-irradiation measured by reverse-phase HPLC equipped with a UV detector (LC/UV). (A) LC/UV chromatograms obtained from non-irradiated cells (upper panel) or cells at 24 h after X-irradiation (lower panel). After X-irradiation at 10 Gy, cells were incubated for 12 or 24 h and collected. Intracellular AMP, ADP, ATP, NAD^+ and NADH levels were measured by HPLC. Representative chromatograms of three experiments are shown. (B) Time course of the intracellular AMP (▲), ADP (■), and ATP (♦) levels as well as adenylate energy charge (AEC; ●). AMP, ADP, and ATP levels were calculated from the calibration curve created by the measurements of standards. AEC was calculated by the following equation: AEC = ([ATP] + 0.5[ADP])/([ATP] + [ADP] + [AMP]). (C) Effect of oligomycin

on cellular ATP production induced by X-irradiation. Oligomycin (2 ng/mL) was applied to cells for 12 h immediately after X-irradiation. (D) Time course of intracellular NAD^+ (△) and NADH (◊). NAD^+ and NADH levels were estimated from the calibration curve created by the measurements of standards. Data are expressed as means ± SE of three experiments. *$P < 0.05$, **$P < 0.01$ (Student's *t*-test).

Figure 4. Mitochondrial electron transport chain-related substance levels in HeLa cells after X-irradiation measured by ESR. (A) Typical ESR spectra at 103 K obtained from HeLa cells without (upper panel, control) and with 10 Gy of X-irradiation (lower panel, X-rays). After X-irradiation at 10 Gy, cells were incubated for 24 h, ESR spectra were then recorded. (B) Effect of rotenone on ESR signal intensity at g = 2.004 (SQ) in HeLa cells. Typical ESR spectra at 103 K were obtained from rotenone-treated cells without (upper panel, control) and with 10 Gy of X-irradiation (lower panel, X-rays), respectively. For rotenone treatment, rotenone (final concentration 1 μM) was added to the medium immediately after irradiation and cells were incubated for 24 h. The ESR scanning parameters were as follows: 2 mW incident microwave power, 9.05 GHz modulation frequency, 1.0 mT field modulation amplitude, and 50 mT scan range. (C) Relative ESR signal intensity of g = 2.004 obtained in HeLa cells after X-irradiation from three independent experiments are summarized. Data are expressed as means ± SE of three experiments. *$P < 0.05$ (Student's *t*-test).

Figure 5. Measurement of mitochondrial electron transport chain-related substances at 20 K. (A) Typical low temperature ESR spectra at 20 K obtained from

HeLa cells without (upper panel, control) and with 10 Gy of X-irradiation (lower panel, X-rays). (B) Relative ESR signal intensity at g = 1.941 obtained from three independent experiments at 20 K are summarized. Data are expressed as means ± SE for three experiments. N.S., not significant (Student's *t*-test).

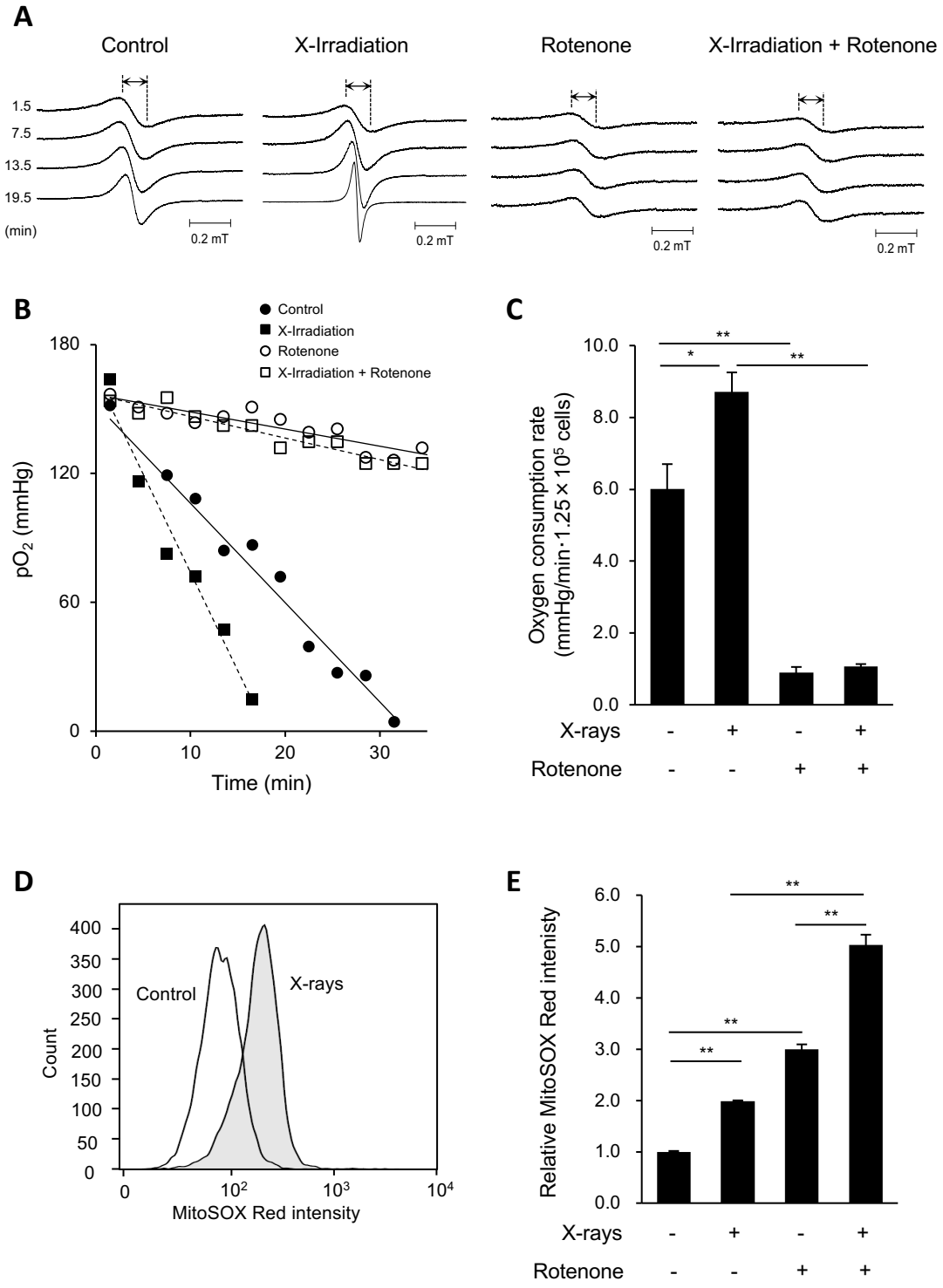

Fig. 1. Yamamoto et al.

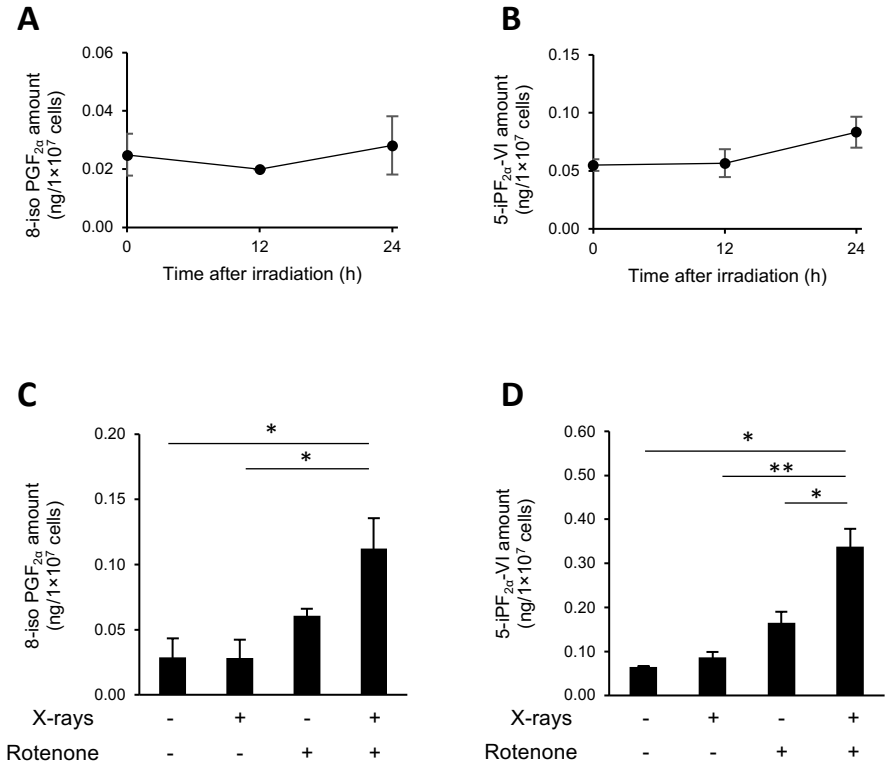

Fig. 2. Yamamoto et al.

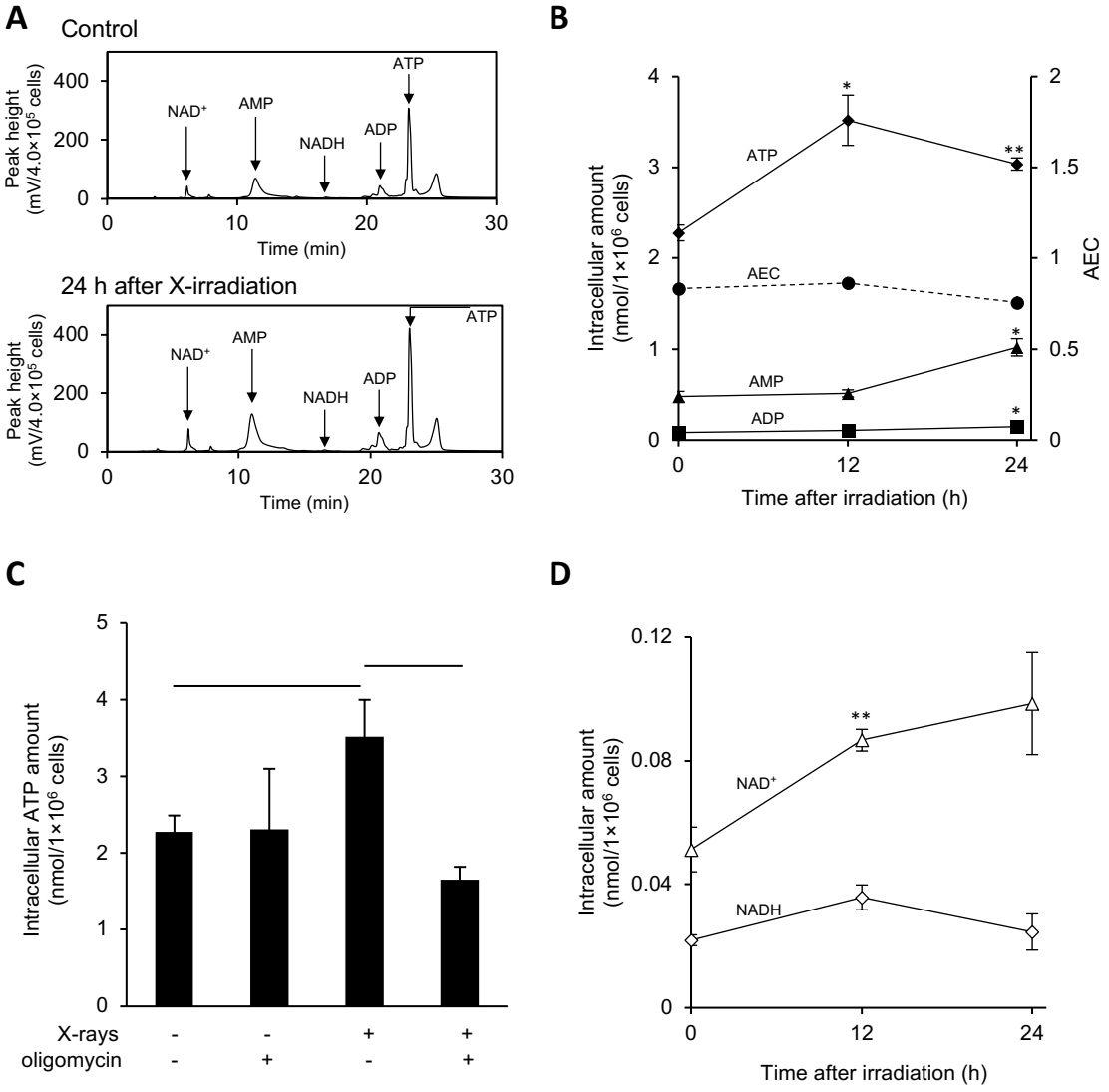

Fig. 3. Yamamoto et al.

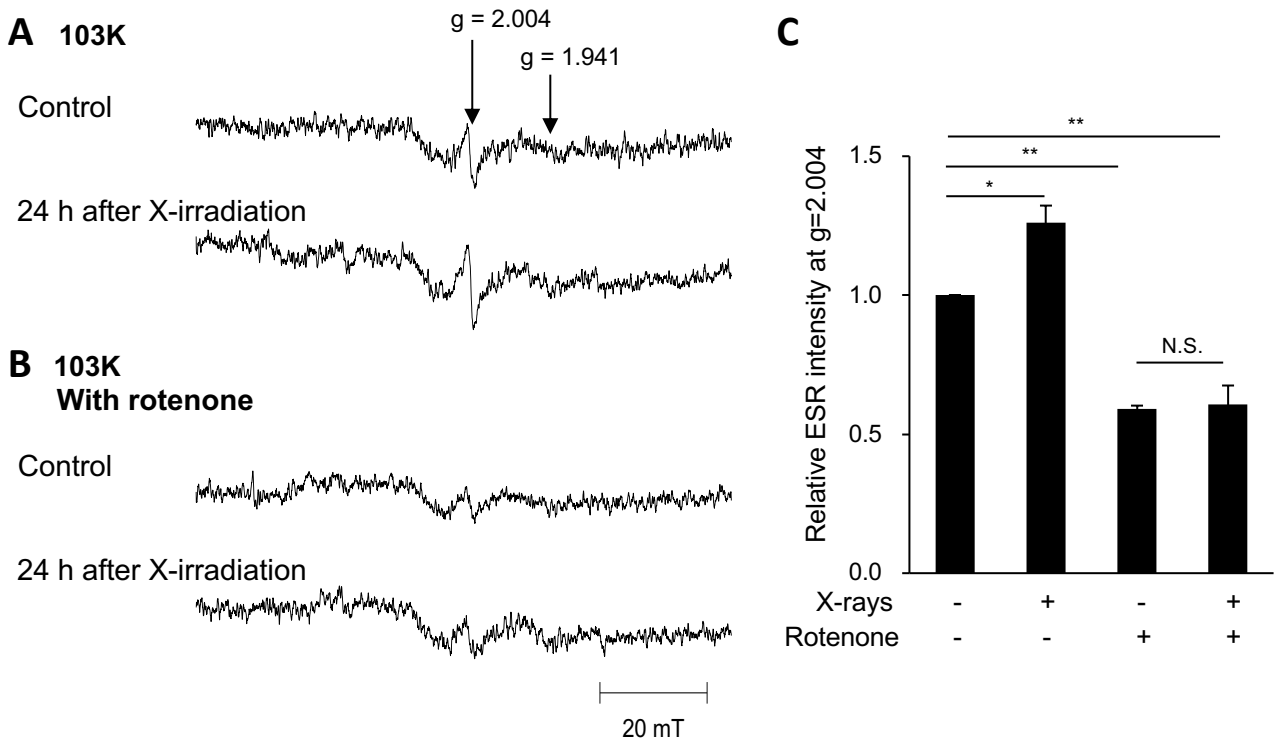

Fig. 4. Yamamoto et al.

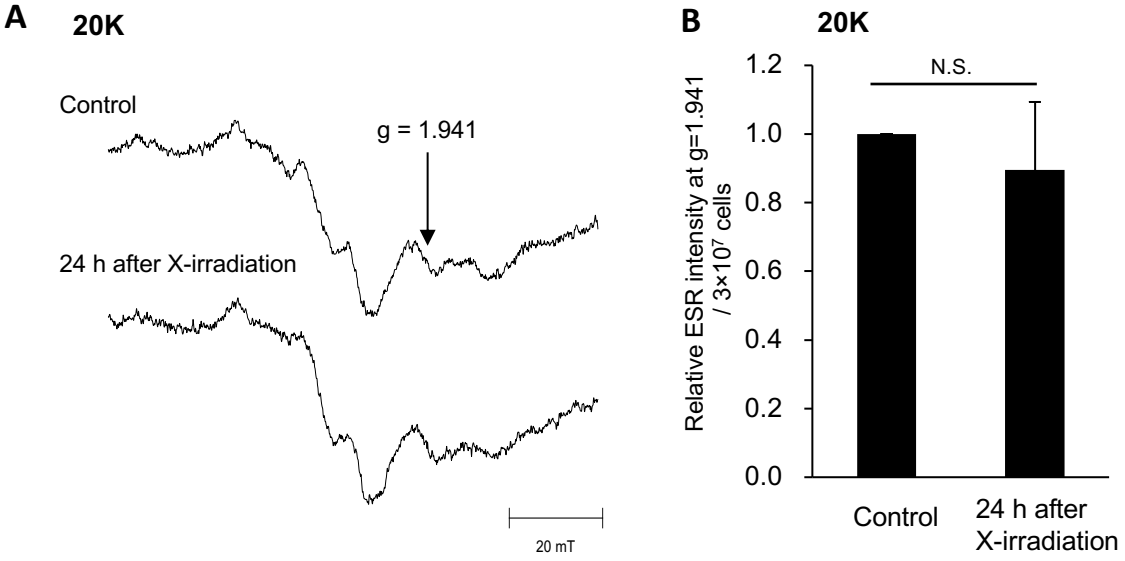

Fig. 5. Yamamoto et al.

Supplementary Materials

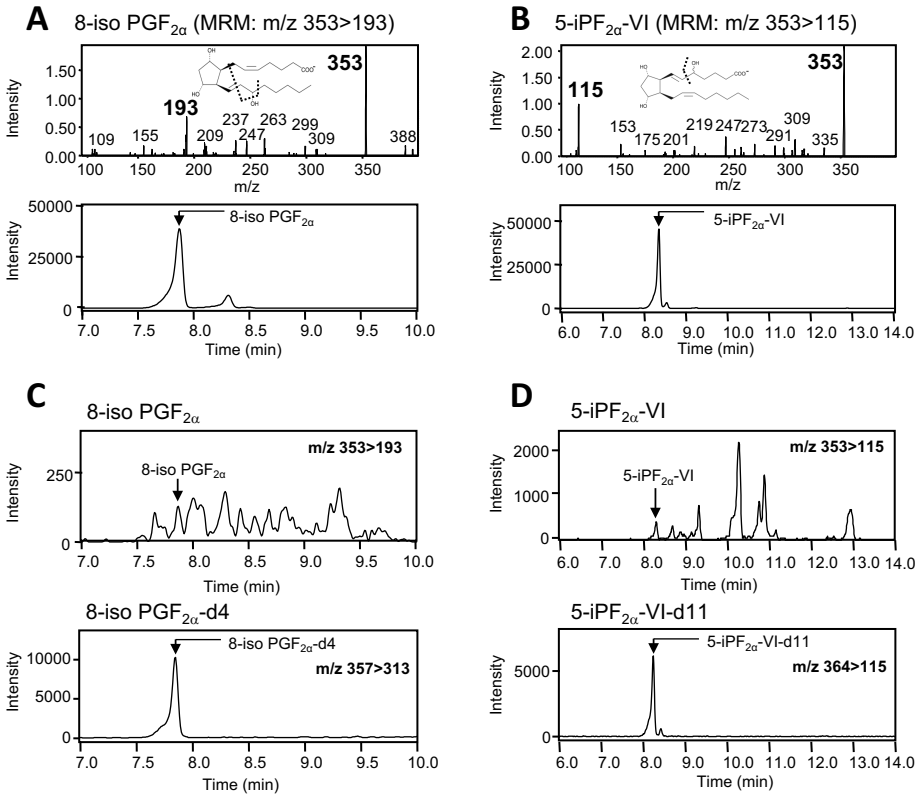

Supplemental Figure 1. LC/MS/MS measurement of cellular F2-isoprostane level in HeLa cells after X-irradiation. (A) Product ion scan (upper panel) and multiple reaction monitoring (MRM) chromatogram (lower panel) of 8-iso $PGF_{2\alpha}$ standard sample (*m/z* 193). (B) Product ion scan (upper panel) and MRM chromatogram (lower panel) of 5-$iPF_{2\alpha}$-VI standard sample (*m/z* 115). (C) LC/MS/MS chromatograms of cellular 8-iso $PGF_{2\alpha}$ (upper panel) or deuterated internal standard (lower panel); 8-iso $PGF_{2\alpha}$-d4 obtained from non-irradiated cells. (D) LC/MS/MS chromatograms of cellular 5-$iPF_{2\alpha}$-VI (upper panel) or deuterated internal standard (lower panel); 5-$iPF_{2\alpha}$-VI-d11 obtained from non-irradiated cells.

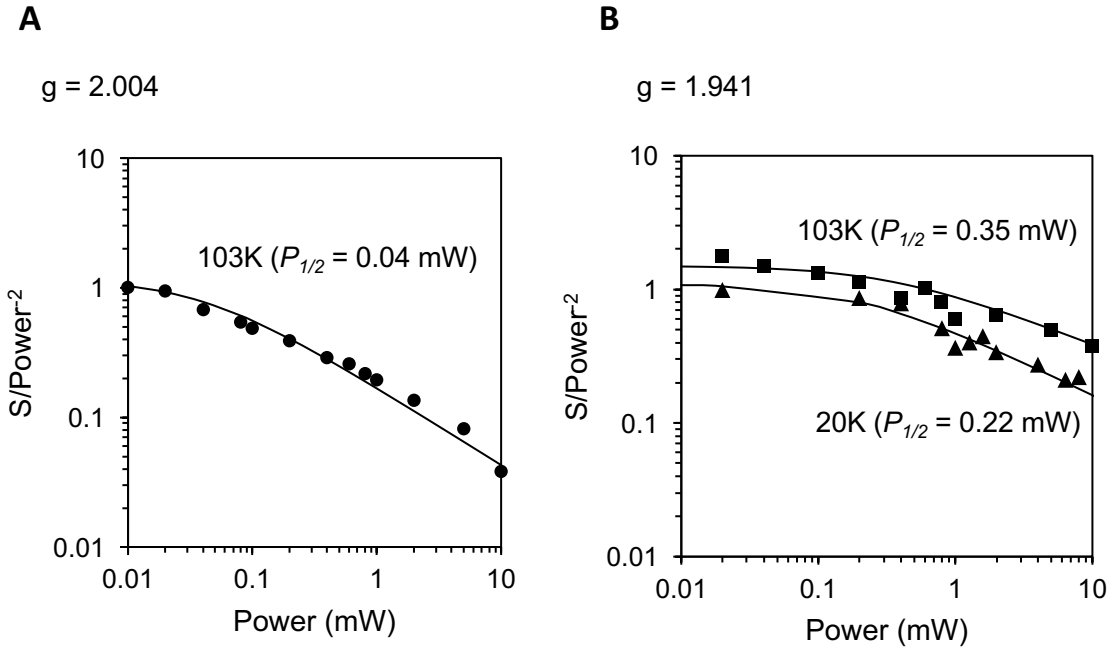

Supplemental Figure 2. Microwave power saturation curves of the ESR signals of HeLa cells at g=2.006 (A) and g=1.941 (B) in HeLa cells. The ESR spectra were measured at various microwave power (0.01~10 mW). Log (Signal amplitude/Power$^{0.5}$) was plotted against log (Power). Padmakumar and Bamerjee [J. Biol. Chem., 270:9295-9300, 1995] have given an equation that the ESR signal amplitude (S) is related to the microwave power (P) by $\log S/(P)^{0.5} = \log A/(1+ P/P_{1/2})^{0.5b}$, where $P_{1/2}$ and A refer to the power for half saturation and a scaling factor, respectively. b refers to the inhomogeneity parameter, which can vary from 1.0 for inhomogenous broadening to 2.0 for homogenous broadening. The value of $P_{1/2}$ was estimated by fitting the experimental saturation data (EPR signal amplitude as a function of incident microwave power) to this equation. Data fitting by a least squares method was performed by a personal computer with Microsoft Excel.